Journal of Electroceramics 5:3, 217–223, 2000
© 2000 Kluwer Academic Publishers. Manufactured in The Netherlands.

Microstructure and Phase Development of Buried Resistors in Low Temperature Co-fired Ceramic

MARK A. RODRIGUEZ, PIN YANG, PAUL KOTULA & DUANE DIMOS
Sandia National Laboratories, P.O. Box 5800, MS 1405, Albuquerque, NM 87185-1405

Submitted December 3, 1999; Revised December 3, 1999; Accepted March 30, 1999

Abstract. Embedded resistor circuits have been generated with the use of a Micropen system, Ag conductor paste (DuPont 6142D), a new experimental resistor ink from DuPont (E84005-140), and Low Temperature Co-fired Ceramic (LTCC) green tape (DuPont A951). Sample circuits were processed under varying peak temperature ranges (835°C–875°C) and peak soak times (10 min–720 min). Resistors were characterized by SEM, TEM, EDS, and high-temperature XRD. Results indicate that devitrification of resistor glass phase to Celcian, Hexacelcian, and a Zinc-silicate phase occurred in the firing ranges used (835–875°C) but kinetics of divitrification vary substantially over this temperature range. The resistor material appears structurally and chemically compatible with the LTCC. RuO_2 grains do not significantly react with the devitrifying matrix material during processing. RuO_2 grains coarsen significantly with extended time and temperature and the electrical properties appear to be strongly affected by the change in RuO_2 grain size.

Keywords: microstructure, buried resistor, LTCC, XRD, SEM

Introduction

The oxide-based thick film resistors are ceramic nanocomposites. Typically these resistors are prepared by screen-printing of a suitable resistor paste onto a dielectric substrate. The resistor paste consists of a fine-grained conductive oxide powder (such as RuO_2) mixed with larger, nonconductive glass particles and an organic vehicle that provides proper rheology for screen-printing. The printed pattern then goes through a drying and firing process where the organic material gradually burns out yielding a stable adherent layer whose microstructure and electrical properties are interrelated. Therefore, precise control of the heat treatment is critical to achieve high tolerance.

Recent trends in high degree integration of passive components for component miniaturization demand the movement of all passive components inside of a multilayer structure. With the development of co-fired ceramic technology, buried components such as resistors, capacitors and inductors can be directly integrated with a single firing step. However, challenges accompanying this development have emerged, namely the physical and chemical compatibility between different materials involved during high temperature co-firing process. The critical issues concerning the physical compatibility are the differential shrinkage and thermal expansion mismatch of buried materials with the dielectric tape (we shall refer to dielectric material as the low temperature co-fired ceramic, or LTCC, throughout the remainder of this manuscript). It is important to select and tailor the material properties to prevent warping and failure of the component during and after the firing process.

Because the conductors, inductors, resistors, and dielectric materials often vary considerably in their chemical makeup, there is also the likelihood of chemical reaction between these materials. The chemical compatibility issues deal with possible chemical reactions between materials in the co-fired structure during high temperature sintering. Since the electrical properties of the functional components may be sensitive to the small variations in composi-

tion as well as new phase and microstructure development, a fundamental understanding of the chemical reactions within and between material components is important in order to control the final properties of the components. This is especially true for buried components where trimming of components is not a viable option. Hence, compatibility issues are paramount for commercial viability and continued industrial growth of this technology.

Garino et al. has reported on physical compatibility issues concerning the LTCC and silver conductor inks [1]. Recently, we have reported on the behavior of the LTCC devitrification kinetics for the Dupont A951 green tape and have briefly summarized the behavior of buried resistors within LTCC [2]. In this paper, we give a more detailed account of the chemical reactions and microstructure evolution for buried resistors in a LTCC multilayer structure, focusing specifically on the new experimental resistor ink from DuPont (E84005-140). This particular resistor ink has been specifically designed for fabrication of buried components using DuPont LTCC tapes. The ink is fabricated using RuO_2 as the conductive phase along with a glassy ''filler'' material. Past investigations of resistor pastes have focused on systems employing a fine grained conductive oxide mixed with a glassy phase [3–5]. In these previous studies, the glassy phase wets the ceramic during firing to provide good mechanical adhesion of the resistor to the LTCC. The glass materials in the resistor and LTCC tape are adjusted to minimize the differential shrinkage during firing to prevent distortion of the fired parts and this is the case for the new experimental ink as well [6]. However, there is one important difference about this new experimental ink that sets it apart from other resistor inks that have been investigated; the glass phase of the new resistor ink devitrifies to a ceramic during processing. The fraction of glass phase that crystallizes is strongly dependent on processing conditions. This is an interesting new variation of the past technology and one that warrants examination. Relick and Ritter [6] of Dupont have discussed the benefits of this new type of resistor system. Their selection of RuO_2 as the conductive oxide was because of its stability in the presence of a surrounding vitreous phase. The selection of a devitrifying matrix in the resistor phase was because it can act as a shield to infiltration of LTCC species during processing, thus limiting reaction and improving control of electrical properties. Additionally, the matching of the devitrification process in the LTCC and resistor phase results in improved structural stability, thus preventing distortion of the fired part.

Experimental Procedure

Sample Preparation

Because our prime interest for this work was to determine the processing-induced changes in material chemistry and microstructure of the thick film resistor materials, special attention was paid to exclude contributions from non-uniform cross-sectional area and thickness variations adjacent to the conductor pads. Since traditional screen-printing produces a thinner layer at the center of a pattern than at the edges, we employed a commercial Micropen system to deposit the resistor pattern onto the LTCC green tape (DuPont A951). Previous results showed that the Micropen is able to precisely control the printed thickness within 3 μm [7]. Since both the resistor and Ag conductor (DuPont 6142D) pastes are compatible with LTCC green tape, the resistor pattern was deposited before the conductor traces were laid down to minimize the resistor thickness variations close to the conductor pattern. The resistor design gives an aspect ratio of 1.2 : 1, with a width of 50 mils (0.127 cm). A total of six layers of green tape were used to build the test circuits. The printed pattern, containing 20 resistors, was deposited on the second layer from the top surface and electrical connections were made through conductor filled via holes. The six layers of the green tape structure were cross-laminated under hydrostatic pressure (3000 psi) at 68°C. After lamination, the samples were fired in a box furnace. The heating rate was controlled at 5°C/min, with a two-hour soak at 450°C to burn out the organics. Samples were fired between 835 and 875°C for various hold times to study the effect of thermal treatment on microstructure and properties. After firing at peak temperature, samples were furnace cooled to room temperature. The room temperature sheet-resistance values of the test resistors were determined by a four-point measurement from the digital multimeter (HP 3457A). Resistance data were reported as the average value of 20 measured resistors.

Characterization

In-situ high-temperature X-ray diffraction analysis was performed using a Scintag X_1 powder diffractometer equipped with Cu Kα radiation, a Peltier-cooled solid-state Ge detector, and a Buehler HTK 1.6 high-temperature furnace. Samples were prepared by depositing a $\sim 40\,\mu$m layer of resistor paste on 9 mm^2 alumina substrates. These samples were heated to various soak temperatures between 835°C and 875°C. At the desired soak temperature, a series of diffraction scans was collected to monitor the crystallization behavior of the resistor material.

Scanning electron microscopy (SEM) was performed on cross-sectioned embedded circuits. Samples were mounted in epoxy, polished smooth, and graphite-coated in preparation for analysis. SEM was performed using a Hitachi S4500 field emission gun (FEG), high-resolution SEM. Energy dispersive spectroscopy (EDS) was carried out using a PGT 60 mm^2 prism detector and Imix software system. SEM and EDS data were collected using a 25 kV acceleration voltage.

Transmission electron microscopy (TEM) was performed using a Philips CM30 microscope operated at 300 kV and equipped with a Link windowless energy-dispersive X-ray spectrometer (EDS) and a Gatan imaging filter capable of imaging with energy-loss electrons. Specimens were prepared for TEM by grinding away one surface of the buried resistor to expose it and then dimpling from the opposite side to less than 15 μm total thickness. Ion thinning was then used to produce an electron transparent foil ($<$200 nm thick) from just the buried resistor material. Phases were identified using electron diffraction patterns, EDS, and energy-filtered imaging. Energy-filtered imaging is capable of showing the spatial distribution of elements in the specimen including boron while the EDS can simultaneously show all the elements detected from a single point.

Results and Discussion

The typical processing conditions for the resistor ink and LTCC are 850°C for $\sim$ 20 min as recommended by the manufacturer. Under these conditions, our diffraction data indicates that the glassy phase in the resistor is roughly half crystallized. Our electrical measurements on samples processed at 850°C for $\sim$ 20 min indicated that the sheet resistance values of resistor pads were similar and did not show a high degree of variation under typical processing conditions. Our selection of peak time and temperature ranges in this study extends beyond the manufacturer's specifications. Extending these processing time/temperature ranges was necessary to obtain the trends that were needed to specifically understand these materials and their interactions from a mechanistic viewpoint. This analysis also serves to determine the extent of valid firing ranges as well as what behaviors can be expected for samples processed outside of these parameters (e.g., a sample that requires multiple firings and hence a longer overall soak time at peak temperature). Table 1 reports observed resistance values for embedded resistors processed under largely contrasting conditions. Although it is not the purpose of this paper to detail electrical measurements on resistors, Table 1 points out the need for a clear understanding of the resistor material behavior during processing to help understand the variation in observed properties. A separate manuscript will give a complete discussion of the electrical properties (resistance, TCR) of these embedded resistors [8].

Initial X-ray Radiography experiments on the imbedded resistors indicated that the resistors were structurally compatible with the LTCC [2]. SEM analysis of cross-sectioned resistors confirmed this initial observation. Figure 1 illustrates a back-scattered electron (BSE) image for a cross-sectioned resistor embedded in LTCC. This sample was fired to 875°C for 40 min; well outside the standard processing range. From this image one can see that there are clearly defined boundaries between the resistor and LTCC and very little observed porosity. In addition, the resistor maintains good mechanical adhesion to the LTCC, without a large degree of reactivity. The image shows the presence of dark and light contrast regions within the LTCC. EDS analysis within a

Table 1. Resistance values for embedded resistors under various process conditions

Processing conditions for sample	Resistance (Ω/sq.)
835°C (10 min)	646.22 ± 22.70
875°C (60 min)	396.76 ± 12.99
875°C (720 min)	1261.69 ± 93.59

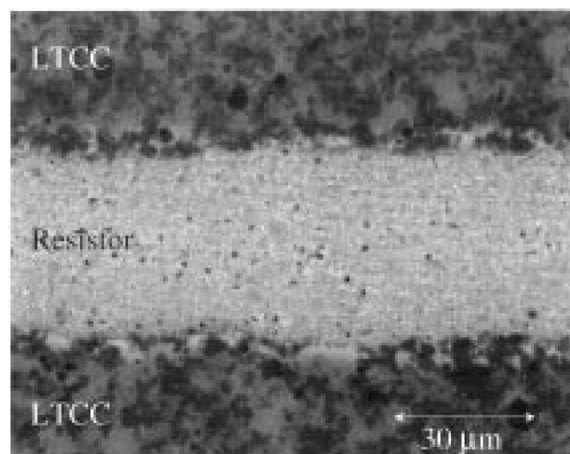

Fig. 1. Back-scattered electron image for a cross-sectioned resistor embedded between layers of LTCC.

region of the LTCC material that encompassed both light and dark contrast regions detected the presence of Al, Ca, Si, Pb, and O with traces of Co, Cr and K. The darker contrast region was identified as alumina while the light contrast was either glass or a crystalline Anorthite phase that devitrified from the glassy material. The resistor displays a brighter appearance due to the higher Z material present. EDS analysis within the region of the resistor material observed a high presence of Ba, Al, Si, Ru, Zn, K, Bi and O as well as traces of Pb, Zr, and Co. The presence of B in the resistor phase was indirectly inferred via microprobe analysis and was later confirmed by energy filtered imaging during TEM analysis. There appears to be a ''halo'' of bright contrast around the resistor that moves into the LTCC. EDS analysis of the halo region showed an increased presence of Bi that accounts for the bright halo effect. Based on the appearance of the microstructure at this interface and the chemical content of the resistor compared to that of the LTCC, it was concluded that the Bi diffused from the resistor into the LTCC. This halo region likely contributes to the good mechanical adhesion between the materials. A previous investigation [7] considered thickness and interfacial effects regarding this system. In that previous study we observed the resistance to be sensitive to the resistor thickness (due to the reaction layer) only when the interface layers contributed a significant fraction of the resistor [7]. This effect occurred for resistors thinner than $\sim 20\,\mu$m. In this study, samples were purposely prepared 30 μm in thickness to minimize the interface effects on resistance. Hence, the reaction layer should not play an important role in the conductivity values observed for these samples. The fact that there is a clear boundary between resistor and LTCC in Fig. 3 illustrates the lack of strong reactivity between the LTCC and resistor phase, affirming the initial motivation of crystallized species in the resistor ''locking-out'' reaction with LTCC species [6]. These observations imply that the resistance variability observed in Table 1 is due almost entirely to the material behavior of the resistor ink during processing.

XRD analysis of the starting materials (not shown) for the resistor ink and LTCC indicated that both of these materials contained a large degree of amorphous (glassy) material. The LTCC exhibited a large amorphous background along with diffraction peaks from crystalline Al_2O_3. Presumably, the additional chemistry observed in the LTCC is tied up in the glass phase. This same situation is true for the resistor ink. XRD data exhibited a large amorphous background along with diffraction peaks from the nanocrystalline RuO_2. There was also a trace of alumina present as well, but for the most part, the additional chemistry (Ba, Al, Si, Zn, K, Bi, Pb, Zr, Co, and B) appeared to be present within the glass phase.

High temperature diffraction analysis was performed to investigate the devitrification behavior of the resistor ink. Figures 2(a) and 2(b) show high-temperature diffraction data for samples fired at 835°C and 875°C, respectively. Both samples were held at peak temperature for 42 min while XRD patterns were collected (6 min each) during the sample divitrification process. Comparison of these two samples shows some rather interesting results. In Fig. 2(a), the sample displays the presence of RuO_2, both a monoclinic and hexagonal phase of the Celcian-type structure. In the 875°C sample, the diffraction peak positions and observed crystallized phases look essentially the same but with some important differences. First, the kinetic behavior of the devitrification process is much faster at 875°C than at 835°C. The sample processed at 875°C shows nearly complete divitrification within 20 min, while the 835°C sample is still only partially crystallized after 40 min of soak time. Hence the 835°C sample would be expected to still have a significant fraction of glass phase remaining even after 40 min while 875°C should be almost entirely crystalline within half that time.

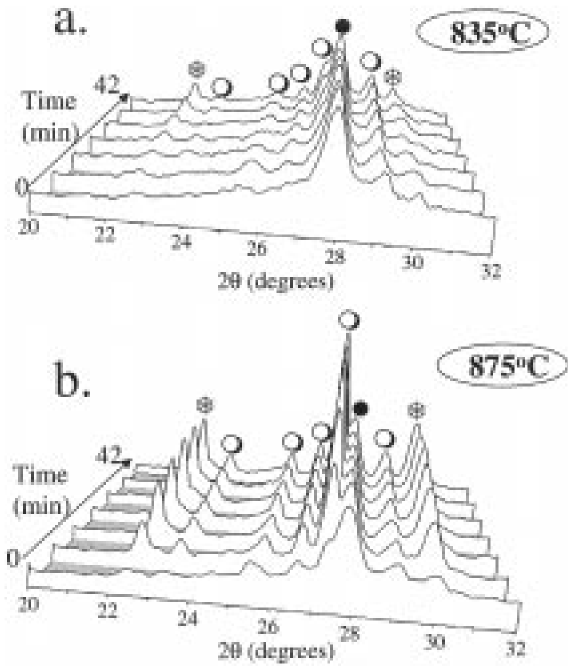

Fig. 2. High Temperature XRD data for resistor ink processed at (a) 835°C and (b) 875°C. (●) identify RuO_2 peaks, (❍) identify monoclinic Celcian peaks, and (❆) identify hexagonal Celcian peaks.

TEM analysis of samples processed under differing conditions matched the XRD observations. Figure 3 shows a TEM micrograph of a region within an embedded resistor. This sample was processed at 835°C for 10 min. Figure 3 shows a large glassy region in the middle of the photo that was caught only part-way through the devitrification process. One can see dendritic grains of Celcian phase growing into the glassy region. Very small grains of RuO_2 are visible at the grain boundary of the large glassy region. Figure 4 shows a TEM micrograph of an embedded resistor that was processed at 875°C for 60 min. This image was taken at higher magnification and focused in on a region near the grain boundaries. In this figure, one can see large grains of the Celcian phase, clusters of RuO_2 grains, and small pockets of glass. Energy filtered imaging indicated a high Zn concentration in the lower-right hand corner of the viewed area in Fig. 4. EDS analysis of this region showed the presence Zn, Si, and O (see Fig. 5) along with a very small Ru peak from the surrounding RuO_2 grains. A Cu artifact peak from the instrumental setup is also present. Further investigation of the Zinc-silicate by electron diffraction confirmed the crystalline nature of this material. The crystal structure of this material is currently being investigated.

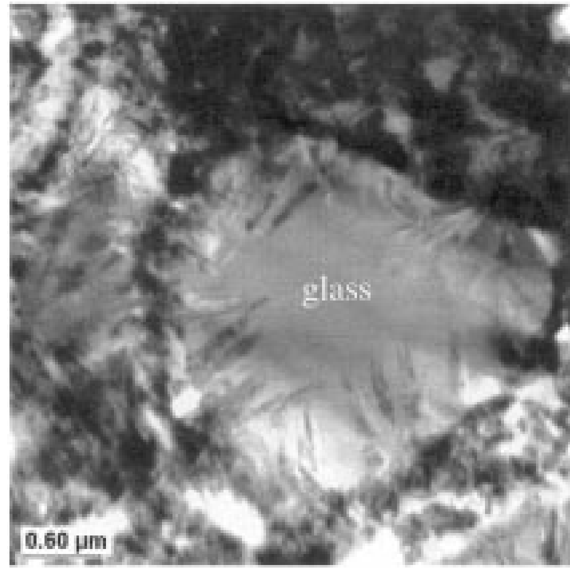

Fig. 3. TEM micrograph of a buried resistor processed at 835°C for 10 min. Sample shows partial devitrification as dendritic Celcian crystals growing at edges of a large glassy particle.

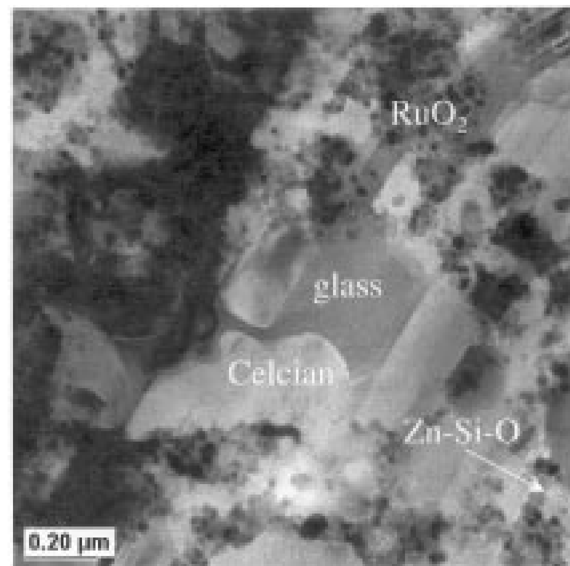

Fig. 4. TEM micrograph of buried resistor processed at 875°C for 60 min. Regions of RuO_2 clusters, large Celcian crystals, residual glass phase, and Zinc-silicate crystals can all be seen in this figure.

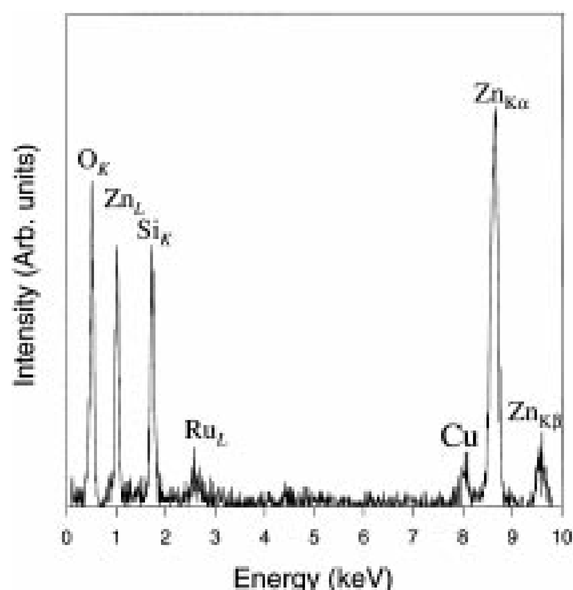

Fig. 5. EDS spectrum of Zn-silicate crystals observed in Fig. 4 confirming presence of Zn, Si, and O. Small Ru peak is from nearby RuO_2 grains. Cu peak is an experimental artifact.

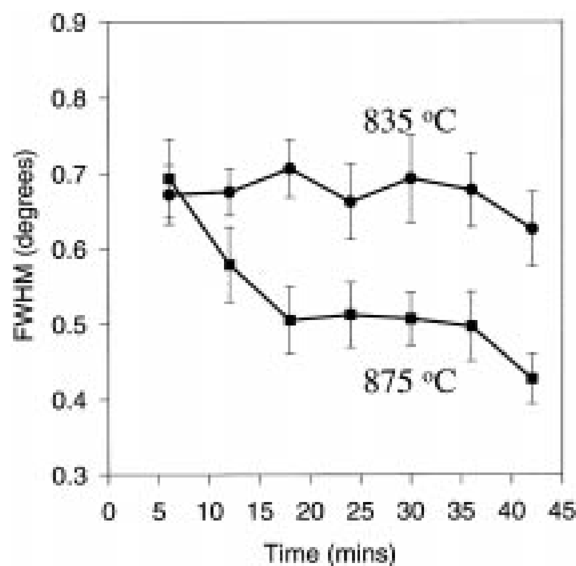

Fig. 6. FWHM of RuO_2 (110) reflection illustrating grain coarsening at 875°C. Error bars are 1σ and are based on redundant profile-fitting calculations performed on the same diffraction pattern.

From initial analysis by TEM, it appeared that the RuO_2 grains coarsened with increased temperature and hold time. If this were true, it was anticipated that the XRD full-width-at-half-maximum (FWHM) of the RuO_2 peaks should decrease in size as the coarsening occurred. Profile-fitting of the diffraction data allowed for a comparison of RuO_2 peak widths. Figure 6 plots the observed FWHM for the RuO_2 (110) peak as a function of time for 835 and 875°C samples. The 835°C sample does not show any significant change in RuO_2 FWHM over the 40 min soak time. However, the 875°C sample shows a significant drop in FWHM. These observations confirm that there is significant RuO_2 grain coarsening occurring as temperature is increased. Crystallite size estimates from these FWHM values indicate that the 835°C sample has a crystallite size near or below 100 angstroms while at 875°C the RuO_2 crystallites have coarsened to ~ 250 angstroms after only 20 min of soak time.

The series of TEM Figs. 7(a), 7(b), and 7(c) clearly demonstrates the coarsening effects of the RuO_2 grains. Figures 7(a), 7(b) and 7(c) were collected on embedded resistor samples that were processed at 835°C for 10 min, 875°C for 60 min, and 875°C for 720 min, respectively. In Fig. 7(a), one sees the very fine RuO_2 grains clustered together. In Fig. 7(b) there is a noticeable increase in RuO_2 grain size within these RuO_2 clusters as compared to Fig. 7(a). When the sample is allowed to soak at 875°C for a very long time as in Fig. 7(c), coarsening is even more evident and the RuO_2 clusters begin to show some discontinuity between grains (i.e., larger inter-granular distance). Another important observation from these figures is that the RuO_2 grains do not appear to be affected chemically by the devitrification process. In contrast, the RuO_2 appears relatively stable in the context of the devitrification process occurring to the remainder of the resistor composition.

When the results of the RuO_2 grain growth from Figs. 6 and 7 are compared to the resistance values as shown in Table 1, we see that the resistance value actually drops with initial coarsening but increases upon further RuO_2 grain growth. The electrical results are strongly dependent on the RuO_2 grain size and separation distance. Pike and Seager have employed a tunneling-barrier model to successfully describe the electrical conduction mechanisms in thick film resistors [9]. We have successfully modeled the resistance and temperature co-efficient of resistance (TCR) behavior of these embedded resistors using a modified form of this tunneling-barrier model, the results of which shall appear in a future manuscript [8].

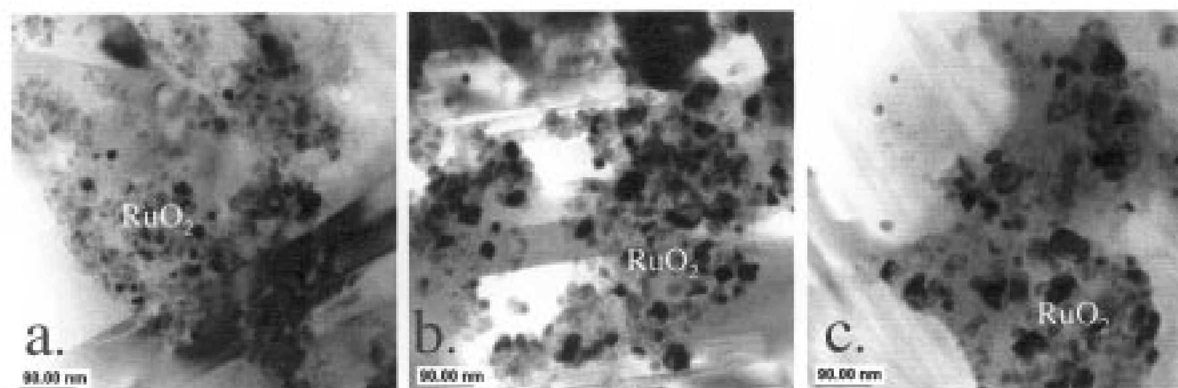

Fig. 7. TEM micrographs showing RuO_2 grain coarsening. Processing conditions for samples were (a) 835°C for 10 min, (b) 875°C for 60 min, (c) 875°C for 720 min.

Conclusion

Characterization of buried resistors by SEM, TEM, EDS, and high-temperature XRD has revealed several important conclusions. First, the resistor material appears structurally and chemically compatible with the LTCC. The new experimental resistor ink demonstrated good mechanical adhesion, limited chemical reaction at the interface (well defined boundaries), low porosity, and no observed cracking due to expansion mismatch or differential shrinkage. Second, the RuO_2 grains do not significantly react with the devitrifying matrix material during processing, but remain relatively inert to the surrounding resistor matrix. Finally, the RuO_2 grains coarsen significantly with extended time and temperature beyond the manufacturers recommended processing conditions as illustrated by TEM micrographs and the FWHM of RuO_2 peaks in XRD patterns. The electrical properties appear to be strongly affected by the change in RuO_2 grain size during processing.

Acknowledgment

The authors would like to acknowledge Alice Kilgo for help with sample preparation, Bonnie McKenzie for SEM/EDS analysis, and Chuck Hills for TEM sample preparation. Sandia is a multiprogram Laboratory operated by Sandia Corporation, a Lockheed Martin Company, for the United States Department of Energy under Contract DE-AC04-94AL85000.

References

1. T. Garino, M.A. Rodriguez, and D. Dimos, *J. Amer. Ceram. Soc.*, (2000).
2. M.A. Rodriguez, P. Yang, P. Kotula, and D. Dimos, *Adv. X-ray Anal.*, **43**, 332 (2000).
3. G.M. Crosbie, F. Johnson, and W. Trela, *J. Appl. Phys.*, **84**, 2913 (1998).
4. B. Morten, A. Masoero, M. Prudenziati, and T. Manfredini, *J. Phys. D: Appl. Phys.*, **27**, 2227 (1994).
5. R.W. Vest, *IEEE Trans. Compon. Hybrids ad Manufact. Technol.*, **14**, 397 (1991).
6. J.R. Rellick and A.P. Ritter, *Int. Conf. On High Density Packag. & MCMs.*, 1–5 (1999).
7. P. Yang, D. Dimos, M.A. Rodriguez, R.F. Huang, S. Dai, and D. Wilcox, ''Direct-Write Percision Resistors for Ceramic Packages,'' in *Materials Research Society Symposium Proceedings* Vol. 542 (Ceramic Freeform and Layered Direct Fabrication, Materials Research Society, Pittsburgh, PA, 1999), pp. 159–164.
8. P. Yang, M.A. Rodriguez, P. Kotula, B.K. Miera, and D. Dimos, *J. Appl. Phys.*, (2000).
9. G.E. Pike and C.H. Seager, *J. Appl. Phys.*, **48**, 5152 (1977).